

Flocking dynamics mediated by weighted social networksJaume Ojer  and Romualdo Pastor-Satorras *Departament de Física, Universitat Politècnica de Catalunya, Campus Nord, 08034 Barcelona, Spain*

(Received 18 May 2022; accepted 14 September 2022; published 3 October 2022)

We study the effects of animal social networks with a weighted pattern of interactions on the flocking transition exhibited by models of self-organized collective motion. We consider variations of traditional models of collective motion in which interactions between individuals are mediated by static complex weighted networks, representing patterns of social interactions. For a model representing dynamics on a one-dimensional substrate, application of a heterogeneous mean-field theory provides a phase diagram as function of the heterogeneity of the network connections and the correlations between weights and degree. In this diagram we observe two phases, one corresponding to the presence of a transition and other to a transition suppressed in an always ordered system, already observed in the nonweighted case. Interestingly, a third phase, with no transition in an always disordered state, is also obtained. These predictions, numerically recovered in computer simulations, are also fulfilled for the more realistic Vicsek model, with movement in a two-dimensional space. Additionally, we observe at finite network sizes the presence of a maximum threshold for particular weight configurations, indicating that it is possible to tune weights to achieve a maximum resilience to noise effects. Simulations in real weighted animal social networks show that, in general, the presence of weights diminishes the value of the flocking threshold, thus increasing the fragility of the flocking state. The shift in the threshold is observed to depend on the heterogeneity of the weight pattern.

DOI: [10.1103/PhysRevE.106.044601](https://doi.org/10.1103/PhysRevE.106.044601)**I. INTRODUCTION**

The self-organized behavior of different interacting animals [1] can lead to complex patterns of movement covering widely separated time- and length scales. Such processes, broadly known as collective motion [2], show stunning examples ranging from the migration of large mammals, the marching of huge groups of desert locusts or the complex and coordinated maneuvering of flocks of birds and shoals of fish, to the swimming and swarming of bacteria [2–6]. The field of collective motion has experienced recently an important boost due to improvements in image acquisition and, especially, in tracking technologies, capable to reconstruct the movement of many unmarked individuals from digital recordings [7,8]. However, most of the scientific effort in the field has had a theoretical nature, based in the study of different representative models [4]. Despite the different formulations of models of collective motion, they are usually based in a set of moving self-propelled particles (SPPs) implementing three main ingredients: (i) avoiding collisions, (ii) trying to stay together, and (iii) trying to align the velocity with that of the nearest neighbors [9–11].

Most of these models consider metric interactions, where the neighbors of the SPPs are defined in terms of Euclidean distance. It has been also proposed that interactions might have in some cases a nonmetric nature, defined by a fixed number of closest neighbors, independently of their relative distance [12,13], and even by a single closest neighbor in the forward direction [14]. These local, metric, or nonmetric rules, however, neglect the effect of possible *social*

interactions among the group members [15] and that can induce individuals to try to follow with higher preference a fixed set of other individuals that are closely connected socially with them [16].

The effect of social interactions in collective motion has been studied in some detail in several models of collective motion [17–27]. Among those models, it plays a prominent role the celebrated Vicsek model [28] defined in terms of a set of SPPs moving in a two-dimensional space. Dynamics evolves in discrete time and is given by the SPPs trying to align the direction of their velocity with the average velocity of a set of other SPPs in a local neighborhood. This alignment is hindered by a source of noise of strength η that represents inherent difficulties in gathering the speed of the neighbors or in implementing the resulting average. The interest of this minimal model of collective motion resides in the fact that it exhibits an order-disorder (*flocking*) transition at a threshold value η_c of the noise intensity, separating an ordered phase at $\eta \leq \eta_c$, in which particles move coherently in a randomly chosen average direction, from a disordered phase at $\eta > \eta_c$, in which SPPs behave as uncorrelated persistent random walkers. This model has allowed us to draw useful conclusions and analogies between the collective motion of animals and the well-known features of order-disorder phase transitions in classical statistical mechanics [4,29], besides having been the subject of many variations and modifications implementing possible realistic features of animal behavior [13,24,30,31].

Social interactions are introduced in the context of the Vicsek model in terms of a variation of this model in which interactions among particles are given by a complex network

[32], in which nodes represent individuals and connections among nodes the presence of social interactions between pairs of individuals. In this model velocities are decoupled from the spatial position of the particles, and the set of interacting neighbors of a SPP is fixed and does not change in time, being given by the network adjacency matrix a_{ij} taking value 1 when nodes i and j are socially connected and 0 otherwise. Several works have considered the effects of different network topologies on the flocking transition experienced by the Vicsek model [17–21]. An interesting observation in this context are the effects that a heterogeneous pattern of social interactions, observed in certain animal social networks [33,34], can have on the flocking transition in the Vicsek model. Reference [22] considered heterogeneous complex topologies represented by networks with a degree distribution $P(k)$, defined as the probability that a node is connected to k other nodes (i.e., has degree k), with a power-law form, $P(k) \sim k^{-\gamma}$ [35]. In this case, it was observed that for a degree exponent $\gamma > 5/2$, a standard transition is present, while for $\gamma < 5/2$, the transition is suppressed, being the system in the ordered state, in the thermodynamic limit of infinite network size, for all physical values of the noise strength η . The same particular role of the degree exponent was recovered analytically in Ref. [23] using the scalar version of the Vicsek model proposed by Czirák, Barabási, and Vicsek, the CBV model [36], in which velocity is a real number, instead of a vector in a two-dimensional space. These results are relevant for the understanding of the collective motion in social animals, as they indicate that the flocking phase is more robust against noise effects in the case of a highly heterogeneous pattern of social contacts.

While the consideration of a networked pattern of contacts provides a realistic setting for the influence of social relation in flocking behavior, it still neglects the important fact that social networks have an intrinsic weighted nature [37–39], which reflects the obvious fact that not all social connections have the same strength, in the sense, for example, that a close friend can exert a stronger influence than a casual acquaintance. Such a weight pattern has been shown to have important effects on dynamical processes running on top of it [40–43] and even to be relevant for the efficient transfer of information between social animals [44].

In this paper we explore the effects of a weighted pattern of social contacts on collective motion by considering the flocking transition of the vectorial Vicsek model and the related scalar CBV model when placed on top of a weighted network. We focus in particular in the case of heterogeneous networks, empirically observed in certain animal social networks [33,34], with a degree distribution of the form $P(k) \sim k^{-\gamma}$. The weighted structure is defined by a heterogeneous pattern of weights w_{ij} , a set of real positive numbers representing the strength of the social tie between individuals i and j . For other analysis of other effects of heterogeneity in collective motion see Refs. [45,46]. For the case of the CBV model, and considering a weight pattern depending on the degree of the connected nodes of the form $w_{ij} = w_0(k_i k_j)^\alpha a_{ij}$, where w_0 is a constant fixing the average weight, as observed in many real systems [38], we develop a theoretical approach based in the heterogeneous mean-field theory (HMF) [43,47–50]. The theory provides a phase diagram for the behavior of the flocking transition threshold η_c in the thermodynamic limit as

a function of the degree exponent γ of the degree distribution and the weight exponent α . This phase diagram recovers the results observed in the unweighted case, namely a phase with a true transition at a finite η_c value and a phase where the transition is absent and the system is always ordered. Surprisingly, however, a new phase emerges in which the system is *always* disordered, in the infinite size limit, for any value of η , however small. In this phase, the systems becomes extremely sensitive to the effects of noise, with a flocking phase that can be destroyed even for small values of η . Additionally, in the case of networks of finite size, we observe that the predicted threshold in a given network has a maximum value for a particular weight exponent, which indicates that we can engineer the resilience of the system to external disorder (i.e., maximize η_c) for a particularly chosen weight structure.

These theoretical predictions are confirmed by means of computer simulations of the CBV model. In the case of the Vicsek model, while lacking an explicit theoretical formulation, we observe numerically that the results for the CBV model can be extrapolated by just taking into account the proper physical limits of the noise parameter η in each model. We finally consider the Vicsek model on real animal social weighted networks. We observe that, in real weighted networks, the effect of a weight structure consists in decreasing the transition threshold with respect to the binary, nonweighted network. This indicates that the actual weight structure makes animal social networks more fragile to external noise. While no theory is again available for real networks, we empirically observe that the shift in the threshold observed in weighted networks can be related to the degree of heterogeneity of the weight pattern.

II. MODELS OF FLOCKING DYNAMICS IN WEIGHTED NETWORKS

In this section we describe the implementation on weighted networks of two models of collective motion, the classical Vicsek model [28], in which particles move on a two-dimensional space with a vectorial velocity, and the CBV model [36], which represents individuals moving on a line and characterized by a scalar velocity. In these models, velocity turns out to be decoupled from spatial position, so we choose to keep track only of the former variables.

A. Vectorial Vicsek model

The Vicsek model is defined in terms of a set of N SPPs moving in a two-dimensional space, characterized by a position $\mathbf{r}_i(t)$ and a velocity $\mathbf{v}_i(t)$ at time t . Dynamics is defined in discrete time and velocities are assumed to have a constant modulus, $|\mathbf{v}_i(t)| = v_0$, and are thus determined by the angle $\theta_i(t)$ they form with the x axis, taking the form

$$\mathbf{v}_i(t) = v_0 \cos \theta_i(t) \hat{\mathbf{i}} + v_0 \sin \theta_i(t) \hat{\mathbf{j}}. \quad (1)$$

In the original Vicsek model [28], each SPP i tends to align its velocity parallel to the average velocity \mathbf{V}_i of a set of SPPs in a local neighborhood inside a circle of radius R centered at i . In the case of an unweighted (binary) network, interactions are constant and defined by the nearest neighbors connected to a node. Thus, in terms of the adjacency matrix, the dynamics

of velocities is defined by the synchronous update rule [22]

$$\theta_i(t+1) = \Theta \left[\mathbf{v}_i(t) + \sum_{j=1}^N a_{ij} \mathbf{v}_j(t) \right] + \eta \xi_i(t), \quad (2)$$

where the function $\Theta[\mathbf{V}]$ returns the angle described by a vector \mathbf{V} , $\xi_i(t)$ is random noise uniformly distributed in the interval $[-\pi, \pi]$, and $\eta \in [0, 1]$ is a parameter measuring the strength of the external noise. We notice that, with this definition, the noise strength has a maximum value $\eta = 1$, compatible with a complete randomization of the information provided by the average velocity of the nearest neighbors.

In the case of weighted networks [38], a real positive number w_{ij} is assigned to the edge connecting nodes i and j , representing the strength of the social interaction between individuals i and j . Here we will consider the case of undirected weighted networks, in which $w_{ij} = w_{ji}$, i.e., the influence of node i over node j is exactly the same as that exerted over i by j . When placed on top of a weighted network, we define the Vicsek update rule by

$$\theta_i(t+1) = \Theta \left[\mathbf{v}_i(t) + \frac{k_i \sum_{j=1}^N w_{ij} \mathbf{v}_j(t)}{\sum_{r=1}^N w_{ir}} \right] + \eta \xi_i(t). \quad (3)$$

With this rule, we consider that the average velocity of the neighbors of agent i is computed giving a normalized weight $w_{ij}/[\sum_r w_{ir}/k_i]$ to each neighbor j , where the normalization factor has been chosen as the average weight of all edges incident to i , in such a way that the limit to a constant value $w_{ij} = w_0$ recovers the dynamics in unweighted networks, Eq. (2).

In many real weighted networks, the weight of the edge connecting nodes i and j is found to be a function of the product of the degrees of the connected nodes [38],

$$w_{ij} = w_0 (k_i k_j)^\alpha a_{ij}, \quad (4)$$

α being an exponent characterizing the correlation between weight and degrees. In this case, the interaction rule takes the simplified form

$$\theta_i(t+1) = \Theta \left[\mathbf{v}_i(t) + \frac{k_i \sum_{j=1}^N k_j^\alpha a_{ij} \mathbf{v}_j(t)}{\sum_{r=1}^N k_r^\alpha a_{ir}} \right] + \eta \xi_i(t). \quad (5)$$

The order parameter for the Vicsek model in networks is defined as in the spatial version, namely

$$\phi(\eta) = \lim_{T \rightarrow \infty} \frac{1}{v_0 T N} \sum_{t'=t_m}^{t_m+T} \left| \sum_{i=1}^N \mathbf{v}_i(t') \right|, \quad (6)$$

where t_m is a sufficiently large thermalization time.

B. Scalar CBV model

The scalar CBV model [36] is defined by a set of N SPPs on a one-dimensional substrate, in which particles move with velocity $u_i(t)$. Each SPP i updates its velocity considering the local average velocity U_i of other agents in a neighborhood $[x_i - \Delta, x_i + \Delta]$ surrounding it. This average velocity is modulated by a function $G(U)$ that restricts the individual velocities to remain close to $+1$ or -1 , in order to avoid diverging trajectories. Individual velocities are finally updated

by this modulated local average velocity with the addition of a noise term. For a binary network, the update rule can be defined as [23]

$$u_i(t+1) = G \left[\frac{\sum_j a_{ij} u_j(t)}{k_i} \right] + \eta \xi_i(t), \quad (7)$$

where ξ_i is a uniform random number in the interval $[-1/2, 1/2]$ and $\eta \in [0, \infty)$ gauges the strength of the external noise. For simplicity, the modulating function $G(U)$ is chosen to be the sign function, taking value $G(U) = +1$ when $U \geq 0$ and $G(U) = -1$ otherwise [23]. We notice that, with this prescription, we do not consider the interaction of the velocity of a node with itself.

In the case of a weighted network, the update rule can be easily extended from the Vicsek model, taking the form

$$u_i(t+1) = G \left[\sum_j w_{ij} u_j(t) \right] + \eta \xi_i(t), \quad (8)$$

where we have discarded irrelevant factors due to the nature of the sign function $G(U)$. When the weights have the topological structure given by Eq. (4), the update rule can be further simplified as

$$u_i(t+1) = G \left[\sum_j k_j^\alpha a_{ij} u_j(t) \right] + \eta \xi_i(t). \quad (9)$$

The order parameter is defined in this case as [23,36]

$$\phi(\eta) = \lim_{T \rightarrow \infty} \frac{1}{TN} \sum_{t'=t_m}^{t_m+T} \left| \sum_{i=1}^N u_i(t') \right|. \quad (10)$$

III. HETEROGENEOUS MEAN-FIELD THEORY FOR THE CBV MODEL IN WEIGHTED NETWORKS

The CBV model in weighted networks can be tackled numerically applying the HMF approximation developed in Ref. [23] (see also Ref. [51]). We start by rewriting the update dynamics in terms of the dual velocities u_i^* as

$$u_i^*(t+1) = G \left[\sum_j k_j^\alpha a_{ij} u_j(t) \right], \quad (11)$$

$$u_i(t+1) = u_i^*(t+1) + \eta \xi_i, \quad (12)$$

from where it is easy to see that the dual velocities fulfill

$$u_i^*(t+1) = G \left[\sum_j k_j^\alpha a_{ij} u_j^*(t) + \eta \sum_j k_j^\alpha a_{ij} \xi_j \right]. \quad (13)$$

Due to the sign function G , the dual velocities are spin variables, $u_i^* = \{-1, 1\}$, a fact that greatly simplifies the subsequent analysis. To solve the dynamics of the dual velocities, we apply an HMF approach inspired in Refs. [23,51,52], assuming that all dynamical properties of nodes are a function of their degree alone, in such a way that nodes with the same degree k , defining a degree class, share the same dynamical properties. We define $\rho_k(t)$ as the probability that a randomly chosen node of degree k is in state $+1$ at time t , and $\psi_k(t)$ as the probability that a randomly chosen node of degree k will

flip to the state +1 at time t . These two quantities are related by the rate equation

$$\begin{aligned}\dot{\rho}_k(t) &= -\rho_k(t)[1 - \psi_k(t)] + [1 - \rho_k(t)]\psi_k(t) \\ &= -\rho_k(t) + \psi_k(t),\end{aligned}\quad (14)$$

which, in the steady state $\dot{\rho}_k(t) = 0$, leads to

$$\rho_k = \psi_k. \quad (15)$$

Consider now the dynamics of Eq. (13), where we drop the star superindex to ease notation. The function ψ_k can be computed considering a node i of degree k and computing its probability to flip to a spin value +1. From Eq. (13), this probability is equal to the probability that the argument R inside the sign function G is positive. This argument can be written as the sum of two contributions, $R = R_u(k) + R_\xi(k)$, with

$$R_u(k) = \sum_j a_{ij} k_j^\alpha u_j, \quad R_\xi(k) = \eta \sum_j a_{ij} k_j^\alpha \xi_j. \quad (16)$$

Starting with the second term, it corresponds to a random variable equal to the sum of k random variables $\eta k_j^\alpha \xi_j$ of mean zero and variance $\sigma_j^2 = k_j^{2\alpha} \sigma_0^2$, where $\sigma_0^2 = \eta^2/12$ is the variance of the original noise term ξ_j . In the HMF approximation, the neighbors j are chosen at random in an uncorrelated network [53] with probability $P_n(k_j) = \frac{k_j P(k_j)}{\langle k \rangle}$, depending only on their degree. By the central limit theorem, we can thus see that $R_\xi(k)$ is a Gaussian random variable of mean zero and variance,

$$\sigma^2 = k \sum_{k_j} \frac{k_j P(k_j)}{\langle k \rangle} \sigma_j^2 = k \sigma_0^2 \frac{\langle k^{1+2\alpha} \rangle}{\langle k \rangle}. \quad (17)$$

The factor $R_u(k)$ is more difficult to estimate probabilistically, so we will only consider its average value. $R_u(k)$ is given by the sum of the contributions $k_j^\alpha u_j$ for the nearest neighbors j of node i . Considering that the variable u_j in a node of degree k' takes value +1 with probability $\rho_{k'}$, the average value of $R_u(k)$ is given by

$$\begin{aligned}\bar{R}_u(k) &= k \sum_{k'} \frac{k' P(k')}{\langle k \rangle} k'^{\alpha} [(+1)\rho_{k'} + (-1)(1 - \rho_{k'})] \\ &= k \sum_{k'} \frac{k'^{1+\alpha} P(k')}{\langle k \rangle} [2\rho_{k'} - 1] = k \frac{\langle k^{1+\alpha} \rangle}{\langle k \rangle} q,\end{aligned}\quad (18)$$

where the factor

$$q = \sum_k \frac{k^{1+\alpha} P(k)}{\langle k^{1+\alpha} \rangle} [2\rho_k - 1] \quad (19)$$

plays the role of an effective order parameter, with value $q = 0$ in the disordered state, where $\rho_k = 1/2$, and $q \neq 0$ in the ordered state $\rho_k \neq 1/2$.

The probability ψ_k is thus equal to the probability that $R = R_\xi(k) + \bar{R}_u(k)$ is larger than zero. Since $R_\xi(k)$ is a Gaussian variable of zero mean and variance Eq. (17), we can write

$$\begin{aligned}\psi_k &= \int_{-\bar{R}_u(k)}^{\infty} \frac{1}{\sqrt{2\pi\sigma^2}} e^{-r^2/(2\sigma^2)} dr = \frac{1}{2} + \frac{1}{2} \operatorname{erf} \left[\frac{\bar{R}_u(k)}{\sqrt{2}\sigma} \right] \\ &= \frac{1}{2} + \frac{1}{2} \operatorname{erf} \left\{ \sqrt{k} \frac{\langle k^{1+\alpha} \rangle}{[\langle k \rangle \langle k^{1+2\alpha} \rangle]^{1/2}} \frac{q}{\sigma_0 \sqrt{2}} \right\},\end{aligned}\quad (20)$$

where $\operatorname{erf}(z) = (2/\sqrt{\pi}) \int_0^z e^{-t^2} dt$ is the error function [54]. In the steady state $\psi_k = \rho_k$, so we can compute q self-consistently from Eq. (20) as

$$\begin{aligned}q &= \sum_k \frac{k^{1+\alpha} P(k)}{\langle k^{1+\alpha} \rangle} [2\rho_k - 1] \equiv F(q) \\ &= \sum_k \frac{k^{1+\alpha} P(k)}{\langle k^{1+\alpha} \rangle} \operatorname{erf} \left\{ \sqrt{\frac{k}{2}} \frac{\langle k^{1+\alpha} \rangle}{[\langle k \rangle \langle k^{1+2\alpha} \rangle]^{1/2}} \frac{q}{\sigma_0} \right\}.\end{aligned}\quad (21)$$

The equation $q = F(q)$ has always a solution $q = 0$, since $F(0) = 0$. From the definition of the error function, and considering the interval $q \in [0, 1]$, one can see that $F(1) \leq 1$, $F'(q) > 0$, and $F''(q) < 0$. This implies that $F(q)$ is a monotonically growing, strictly concave function. It thus can only cut the identity line $y(q) = q$, corresponding to a nonzero solution, when the first derivative of $F(q)$ evaluated at $q = 0$ is larger than one, that is, when

$$\begin{aligned}F'(0) &= \sum_k \frac{k^{1+\alpha} P(k)}{\langle k^{1+\alpha} \rangle} \frac{2}{\sqrt{\pi}} \sqrt{\frac{k}{2}} \frac{\langle k^{1+\alpha} \rangle}{[\langle k \rangle \langle k^{1+2\alpha} \rangle]^{1/2}} \frac{1}{\sigma_0} \\ &= \sqrt{\frac{2}{\pi}} \frac{1}{\sigma_0} \frac{\langle k^{3/2+\alpha} \rangle}{[\langle k \rangle \langle k^{1+2\alpha} \rangle]^{1/2}} > 1.\end{aligned}\quad (22)$$

From here, a threshold condition appears,

$$\sigma_0 < \sqrt{\frac{2}{\pi}} \frac{\langle k^{3/2+\alpha} \rangle}{[\langle k \rangle \langle k^{1+2\alpha} \rangle]^{1/2}}, \quad (23)$$

that, in terms of the noise intensity $\eta = \sqrt{12}\sigma_0$, allows us to define the noise threshold

$$\eta_c = \sqrt{\frac{24}{\pi}} \frac{\langle k^{3/2+\alpha} \rangle}{[\langle k \rangle \langle k^{1+2\alpha} \rangle]^{1/2}}, \quad (24)$$

such that an ordered state is present for $\eta < \eta_c$, and a disordered one for $\eta > \eta_c$. We notice here the presence of an erroneous factor 2 in Eq. (29) of Ref. [23], which renders it equal to our general prediction Eq. (24) for $\alpha = 0$ in the limit of large threshold.¹

In the case of interest of scale-free networks with a degree distribution $P(k) \sim k^{-\gamma}$, the value of the noise threshold of the CBV model in weighted networks depends on ratios of moments that can lead to peculiar behavior in the thermodynamic limit depending on α and γ . Assuming $\gamma > 2$, in order to ensure a sparse network with constant average degree $\langle k \rangle$, the value of the threshold depends on the moment ratio $\eta_c \sim \langle k^{3/2+\alpha} \rangle / \langle k^{1+2\alpha} \rangle^{1/2}$. Defining the functions

$$\alpha_N(\gamma) = \gamma - \frac{5}{2}, \quad \alpha_D(\gamma) = \frac{\gamma}{2} - 1, \quad (25)$$

we can see that, in a network with a maximum degree k_c [49,55], the numerator of Eq. (24) diverges in the thermodynamic limit $k_c \rightarrow \infty$ as $\langle k^{3/2+\alpha} \rangle \sim k_c^{\alpha-\gamma+\frac{5}{2}}$ for $\alpha > \alpha_N(\gamma)$, while it goes to a constant for $\alpha < \alpha_N(\gamma)$. On the other

¹In Ref. [23] the term corresponding to the factor $R_u(k)$ in a binary network was treated probabilistically and not in average value. This explains that the result here and there only coincide in the limit of large threshold.

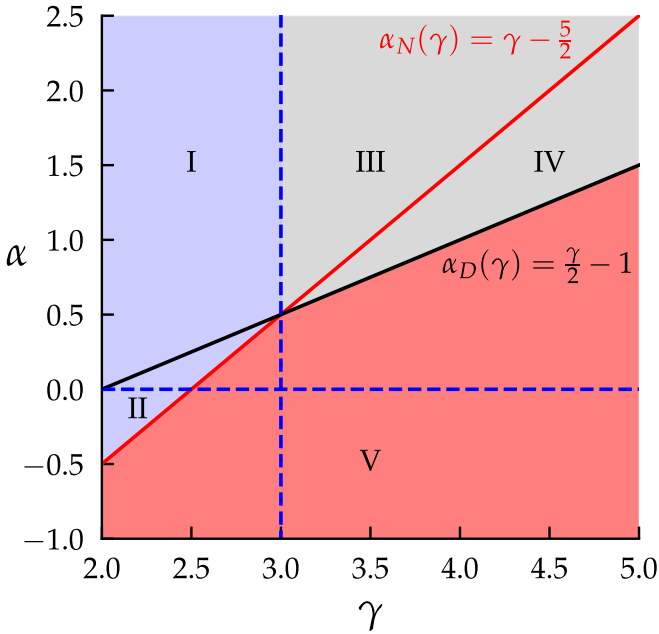


FIG. 1. Phase diagram of the CBV model on weighted networks. Red and black lines mark respectively the functions $\alpha_N(\gamma)$ and $\alpha_D(\gamma)$, defined in Eq. (25). The vertical dashed line indicates the value $\gamma = 3$. The horizontal dashed line indicates the value $\alpha = 0$, corresponding to an unweighted network. In regions I and II (shaded in blue), the threshold diverges in the thermodynamic limit, $\eta_c \rightarrow \infty$; in regions III and IV (shaded in gray), the threshold converges to zero, $\eta_c \rightarrow 0$; in region V (shaded in red), the threshold converges to a constant, $\eta_c \rightarrow \text{const}$.

hand, the denominator diverges as $\langle k^{1+2\alpha} \rangle^{1/2} \sim k_c^{\alpha - \frac{\gamma}{2} + 1}$ for $\alpha > \alpha_D(\gamma)$, going instead to a constant for $\alpha < \alpha_D(\gamma)$. This leads to different scaling behaviors of the noise threshold in the thermodynamic limit that are summarized in the phase diagram portrayed in Fig. 1. In regions I and III, both numerator and denominator diverge, leading to $\eta_c \sim k_c^{(3-\gamma)/2}$. Thus, in region I, with $\gamma < 3$, the noise threshold diverges, while it converges to zero in region III. In region II, numerator diverges and denominator converges, and so the threshold diverges. In region IV, numerator and denominator exchange behavior, and thus the threshold converges to zero. Finally, in region V, both denominator and numerator converge, and the threshold converges to a constant.

The scaling of the threshold with the network size N can be recovered if we consider, for uncorrelated networks, that $k_c \sim N^{1/2}$ for $\gamma < 3$ and that $k_c \sim N^{1/(\gamma-1)}$ for $\gamma > 3$ [56]. We therefore obtain, in the limit of large N and in the different regions:

- Region I: $\eta_c \sim N^{(3-\gamma)/4} \rightarrow \infty$;
- Region II: $\eta_c \sim N^{[2(\alpha-\gamma)+5]/4} \rightarrow \infty$;
- Region III: $\eta_c \sim N^{-(\gamma-3)/[2(\gamma-1)]} \rightarrow 0$;
- Region IV: $\eta_c \sim N^{-[2(\alpha+1)-\gamma]/[2(\gamma-1)]} \rightarrow 0$;
- Region V: $\eta_c \rightarrow \text{const}$.

This analytical solution recovers the main result in Ref. [23] regarding the presence of a phase in which a true

transition is present, characterized by a finite threshold, separated from another region in which the threshold tends to infinity, indicating that the transition is absent and, therefore, the system is always ordered for any value of η . These regions now depend on the values of α for $\gamma < 3$. The most noticeable feature of this solution, however, is the emergence of a new phase, regions III and IV, in which a set of values of α for $\gamma > 3$ lead to a null threshold in the thermodynamic limit. This case corresponds again to the absence of transition, but now in a system that is always in the disordered state, no matter how small the noise strength might be.

IV. NUMERICAL RESULTS IN SYNTHETIC WEIGHTED NETWORKS

In order to check the analytical predictions obtained in the previous section, as well as to obtain a more precise rendering of the effects of a weighted topology on the ordering dynamics of the CBV and Vicsek model, in this section we consider numerical simulations of both models on synthetic heterogeneous networks with a scale-free degree distribution given by a power-law form, $P(k) \sim k^{-\gamma}$. In particular, we generate networks using the uncorrelated configuration model (UCM) [57] with a minimum degree $k_{\min} = 3$ and a maximum degree $k_c = \min(N^{1/2}, N^{1/(\gamma-1)})$, in order to avoid degree correlations and maximum degree fluctuations [55,56]. On these networks, we impose a weight on each edge given by Eq. (4). The parameters of the network models are thus the degree exponent γ and the weight exponent α . In our simulations, we compute statistical quantities allowing for a thermalization time $t_m = 50\,000$ and averaging over $T = 250\,000$ time steps for the CBV model. For the Vicsek model, we choose $t_m = 10\,000$ and $T = 50\,000$.

A. CBV model

In the first place, we check the predictions of the HMF theory developed in Sec. III for the CBV model on weighted networks. In Fig. 2 we show the order parameter $\phi(\eta)$ as a function of the noise intensity η computed in networks of different degree and weight exponents. As we can see from this figure, the order parameter is compatible with the presence of a threshold that depends in a complex way on both exponents γ and α . In order to determine this threshold noise in simulations on necessarily finite systems, we consider the dynamic susceptibility, defined as [58,59]

$$\chi_N(\eta) = N \frac{\langle \phi^2 \rangle - \langle \phi \rangle^2}{\langle \phi \rangle}. \quad (26)$$

The effective critical point $\eta_c(N)$ in a network of size N is given by the value of the noise at the maximum of the susceptibility $\chi_N(\eta)$ [22,23,58,59]. In Fig. 3 we plot the shape of the dynamic susceptibility computed from a sample of values of γ and α . As we can see, a clear peak is observed in all plots that allows us to define the effective threshold as a function of the network size, $\eta_c(N)$. At this peak, the maximum value of the dynamic susceptibility, $\chi^{\text{peak}}(N) \equiv \chi_N[\eta_c(N)]$, is expected to show a power-law increase with the network size,

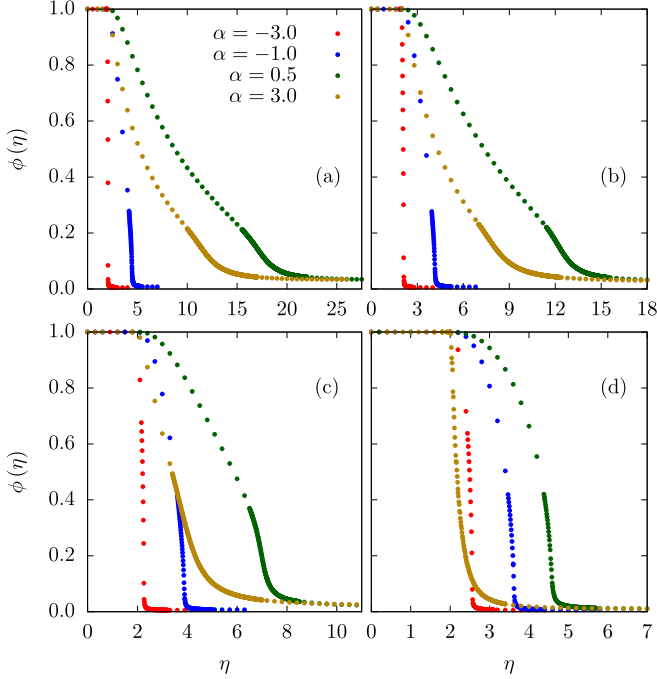


FIG. 2. Order parameter $\phi(\eta)$ as a function of η in the CBV model on weighted UCM networks with different degree (γ) and weight (α) exponents. Panels correspond to different values of the degree exponent: (a) $\gamma = 2.10$, (b) $\gamma = 2.35$, (c) $\gamma = 2.75$, and (d) $\gamma = 3.50$. Network size $N = 10^5$.

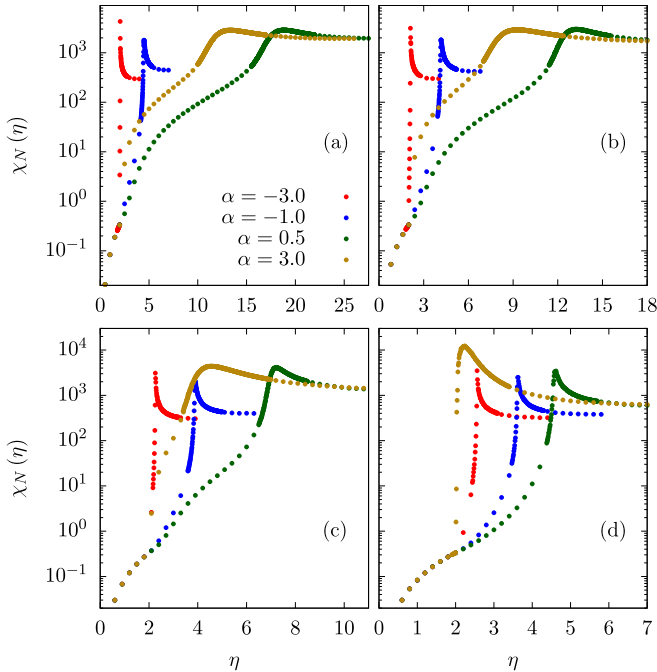


FIG. 3. Dynamic susceptibility $\chi_N(\eta)$ as a function of η in the CBV model on weighted UCM networks with different degree (γ) and weight (α) exponents. Panels correspond to different values of the degree exponent: (a) $\gamma = 2.10$, (b) $\gamma = 2.35$, (c) $\gamma = 2.75$, and (d) $\gamma = 3.50$. Network size $N = 10^5$.

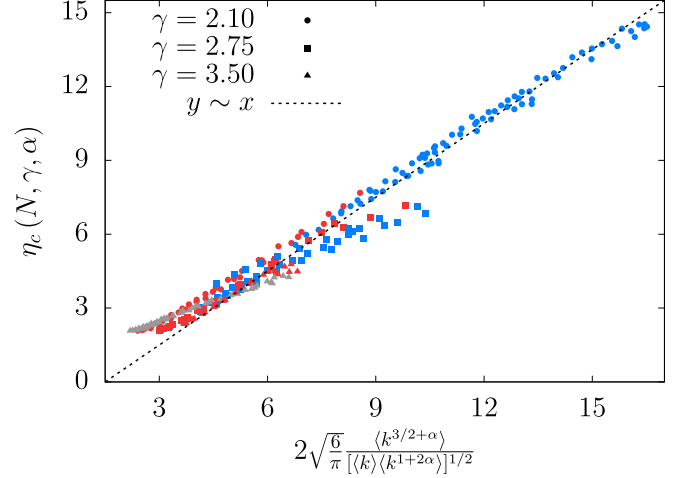


FIG. 4. Effective critical point $\eta_c(N, \gamma, \alpha)$ as a function of the theoretical prediction, Eq. (24), in the CBV model on weighted UCM networks with different degree (γ) and weight (α) exponents and different network sizes N . The values of α and N considered range in the intervals $[-3, 4]$ and $[10^3, 10^5]$, respectively. The color of the symbols denote their position in the phase diagram Fig. 1: blue for regions I and II ($\eta_c \rightarrow \infty$); gray for regions III and IV ($\eta_c \rightarrow 0$); red for region V ($\eta_c \rightarrow \text{const}$).

given by [23,58]

$$\chi^{\text{peak}}(N) \sim N^\delta, \quad (27)$$

where δ is a characteristic exponent.

In Fig. 4 we compare the effective threshold $\eta_c(N, \gamma, \alpha)$ in the CBV model, estimated by the peak of the dynamic susceptibility, with the theoretical HMF prediction in Eq. (24), for different values of the degree exponent γ , weight exponent α , and network size N . As we can see, disregarding a common vertical intercept, the theoretical prediction provides a very good approximation to the numerical values observed in simulations. The fit is particularly good for region I (blue circles) and region V (red symbols), where the threshold is expected to diverge or converge to a constant, respectively, in the thermodynamic limit.

We now verify the scaling behavior of the threshold in the different regions represented in the phase diagram in Fig. 1. To do so, in Fig. 5 (left panels) we plot the effective threshold $\eta_c(\alpha)$, measured as the peak of the dynamic susceptibility, as a function of the weight exponent α in networks of different degree exponent γ , for different network sizes N . From this figure, we can see that the numerical thresholds indeed recover the scaling form resulting from the HMF analysis. For $\gamma = 2.1$, the values of α in region V lead to an effective threshold converging to a constant as we increase the network size. For values of α in regions I and II, on the other hand, the threshold is observed to diverge for increasing N . For $\gamma = 2.75$, small values of α in region V again lead to a constant threshold. However, the situation for larger values of α is more complex, due to the fact that this value of γ is quite close to the singular case of $\gamma = 3$ for which $\alpha_N(\gamma) = \alpha_D(\gamma)$ and all regions coalesce. One would need much larger network sizes to observe the theoretical prediction for the thermodynamic limit. For $\gamma = 3.5$ we recover in region V (small α) a

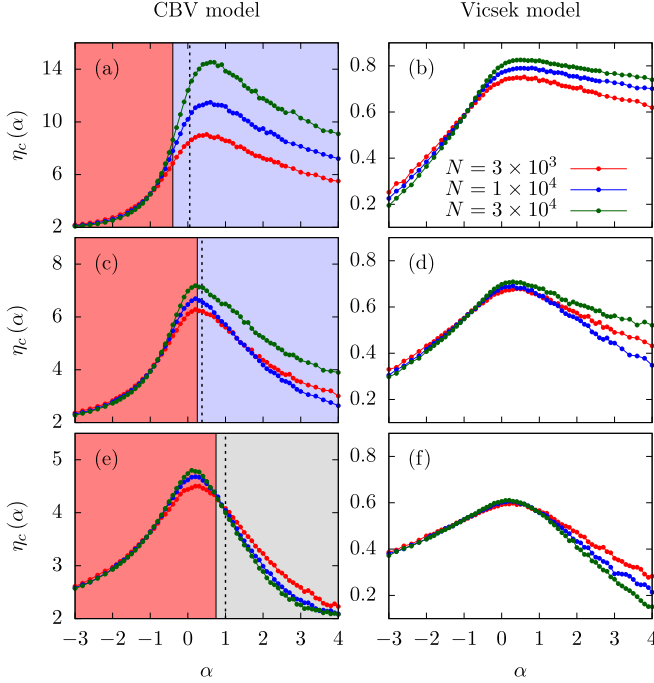


FIG. 5. Effective critical point $\eta_c(\alpha)$ as a function of the weight exponent α on UCM networks of different size N . Left panels show results corresponding to the CBV model. In this case, we have color-marked the region in the phase diagram Fig. 1 corresponding to the expected scaling of the threshold: red (region V) for $\eta_c \rightarrow \text{const}$, blue (regions I and II) for $\eta_c \rightarrow \infty$; gray (regions III and IV) for $\eta_c \rightarrow 0$. Vertical dashed lines mark the transition from region I to II, and from III to IV. Right panels correspond to simulations of the Vicsek model. Values of gamma are [(a) and (b)], $\gamma = 2.10$, [(c) and (d)] $\gamma = 2.75$, [(e) and (f)] $\gamma = 3.50$.

converging threshold. For large α in regions III and IV, however, we observe the interesting feature of a threshold that tends to zero when increasing the network size. Again, finite-size effects affect the behavior in the boundary between regions V and IV.

Another important feature that can be observed from Fig. 5 (left panel) is the presence of a maximum in the threshold $\eta_c(\alpha)$ as a function of α . This maximum reflects the fact that the resilience of the system to the effects of noise is maximal for a weight exponent α_{\max} , depending in principle on the degree exponent. This observation can be recovered analytically by setting equal to zero the derivative of Eq. (24) with respect to α and solving the ensuing equation that leads to $\alpha_{\max}^{\text{HMF}} = 1/2$ for any γ . The threshold at this maximum depends on the second moment of the degree distribution, $\eta_c^{\max} \sim \langle k^2 \rangle^{1/2}$, diverging in the thermodynamic limit for $\gamma < 3$ (region I) and converging to a constant for $\gamma > 3$ (region V). In numerical simulations, Fig. 5 (left panel), the maximum α_{\max} is clearly present, but it seems to depend on the degree exponent and to slightly change with the network size. In order to check this, in Table I we summarize the variation of the maximum $\alpha_{\max}(\gamma)$ estimated numerically as we increase N and depending on the heterogeneity of the network. These numerical results show that HMF analysis provides a very good prediction for small values of the degree exponent, with $\alpha_{\max} \simeq 0.5$ for $\gamma = 2.1$.

TABLE I. Numerical estimation of the weight exponent $\alpha_{\max}(\gamma)$ for which the effective threshold is maximum, $\eta_c^{\max} \equiv \eta_c[\alpha_{\max}(\gamma)]$, in the CBV model on UCM weighted networks of different degree exponent γ and size N . The error in the estimation of the maxima is $\Delta\alpha_{\max} = 0.1$ in all cases.

N	$\alpha_{\max}(\gamma)$			
	$\gamma = 2.10$	$\gamma = 2.35$	$\gamma = 2.75$	$\gamma = 3.50$
3×10^3	0.5	0.6	0.2	0.3
1×10^4	0.6	0.5	0.2	0.2
3×10^4	0.6	0.6	0.2	0.1
1×10^5	0.6	0.7	0.1	0.1
3×10^5	0.5	0.8	0.1	0.1

For larger values of γ we obtain a more complex dependence. Thus, for large N and $\gamma = 2.35$ we have $\alpha_{\max} \simeq 0.7$, while for $\gamma \geq 2.75$ we observe $\alpha_{\max} \simeq 0.1$.

Finally, in Fig. 6 we study in more detail the finite-size scaling of the CBV model as a function of network size N for different points (γ, α) belonging to regions I, III, and V. We do not consider regions II and IV since it is difficult to select points sufficiently away from the boundaries $\gamma = 3$, $\alpha_N(\gamma)$ and $\alpha_D(\gamma)$, without choosing extremely large values of γ and α . In Fig. 6(a) we plot the resulting evolution of the effective threshold as a function of N . The points

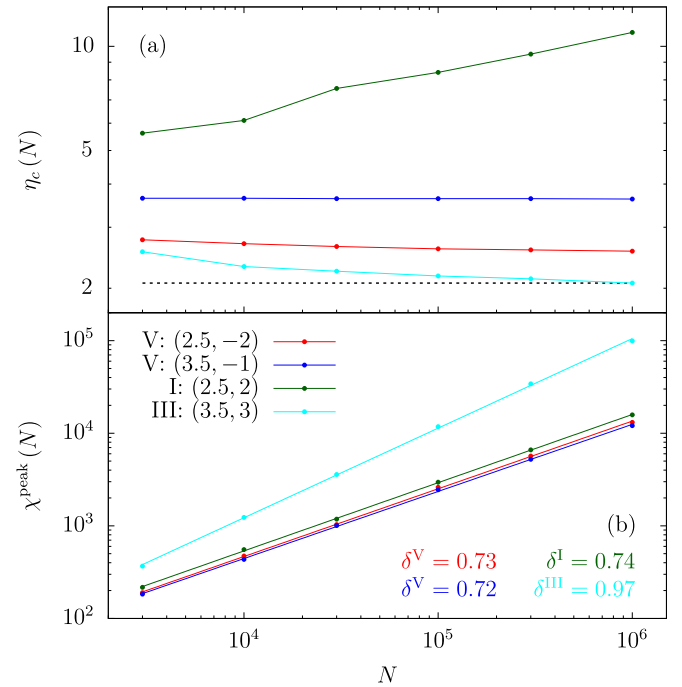


FIG. 6. (a) Effective critical point $\eta_c(N)$ as a function of the network size N for different pairs of values (γ, α) belonging to regions I, III, and V. The dashed horizontal line serves to highlight the slow decay to zero of the threshold observed in region III. (b) Maximum of the dynamic susceptibility at the peak, $\chi^{\text{peak}}(N)$, as a function of the network size N for different pairs of values (γ, α) . The exponents δ quoted of the different regions are obtained by means of a linear regression in log-log scale to the form $\chi^{\text{peak}} \sim N^\delta$. Results correspond to the CBV model on UCM weighted networks.

corresponding to region V show a very clear plateau, indicative that the constant threshold predicted by HMF is quickly reached for moderate network sizes. On the other hand, for the points in regions I and III, the threshold shows an increasing and decreasing trend, respectively. The increase of threshold with N in region I is very clear, while the decrease in region III is weaker. This fact can be understood at the HMF level from the scaling of the threshold as a function of N given in Sec. III. In region I, we have $\eta_c^I(N) \sim N^{(3-\gamma)/4}$, which for our sample point (2.5, 2) leads to $\eta_c^I(N) \sim N^{1/8}$. In region III, instead, $\eta_c^{III}(N) \sim N^{-(\gamma-3)/[2(\gamma-1)]}$, that for the sample point (3.5, 3) yields $\eta_c^{III}(N) \sim N^{-1/10}$, that is, a smaller exponent than that expected in region I. We notice however that, despite this argument is qualitatively correct, our numerical simulation do not recover the exponents predicted by the theory.

In Fig. 6(b) we study the behavior of the maximum value of the dynamic susceptibility at its peak, $\chi^{\text{peak}}(N)$, as a function of N . In accordance with the theoretical expectation, Eq. (27), we observe that the peak of the susceptibility increases with network size as a power law, $\chi^{\text{peak}}(N) \sim N^\delta$. The characteristic growth exponent δ seems to be constant and the same in regions I and V, $\delta \simeq 0.73$, and instead it is quite larger in region III, $\delta \simeq 0.97$.

B. Vicsek model

We have also performed numerical simulations of the vectorial Vicsek model in weighted UCM networks. In this case, we do not have an explicit analytical solution. We can, however, extrapolate the results of the CBV model pursuing the analogy made in the case of binary networks with $\alpha = 0$ [23]. Since the noise intensity is bounded by the maximum value 1 in the Vicsek model, we can interpret the different regions of the phase diagram in the CBV model directly, just considering that regions I and II, where the CBV model exhibits a diverging threshold, correspond in the Vicsek case to a threshold that saturates to the maximum value 1 in the thermodynamic limit.

In Fig. 5 (right panel) we present the evolution of the effective threshold $\eta_c(\alpha)$ in the Vicsek model as a function of the weight exponent α for UCM networks of different degree exponent and size. A comparison with the corresponding plots for the CBV case presented in the left panel shows that both models exhibit the same trend in the behavior of the threshold for different values of α . This indicates that both models have an analogous phase diagram, as long as a diverging threshold in regions I and II in the CBV model is interpreted as a threshold converging to 1 in the Vicsek model. This observation provides further confirmation of the fact that the dimensionality of the order parameter does not play a relevant role in the characterization of the behavior of critical transitions in networks [22,49].

In Fig. 7(a) we show the analogous scaling with network size of the effective threshold of the Vicsek model in the same representative points of the different regions of the phase diagram. As we can see, in full agreement with the observations for the CBV model, region V leads to thresholds saturating to a constant value, region III is characterized by a threshold decreasing with network size, while region I shows an increasing threshold, necessarily saturating to the maximum value $\eta = 1$. Interestingly, the rate of decrease of the threshold in region III

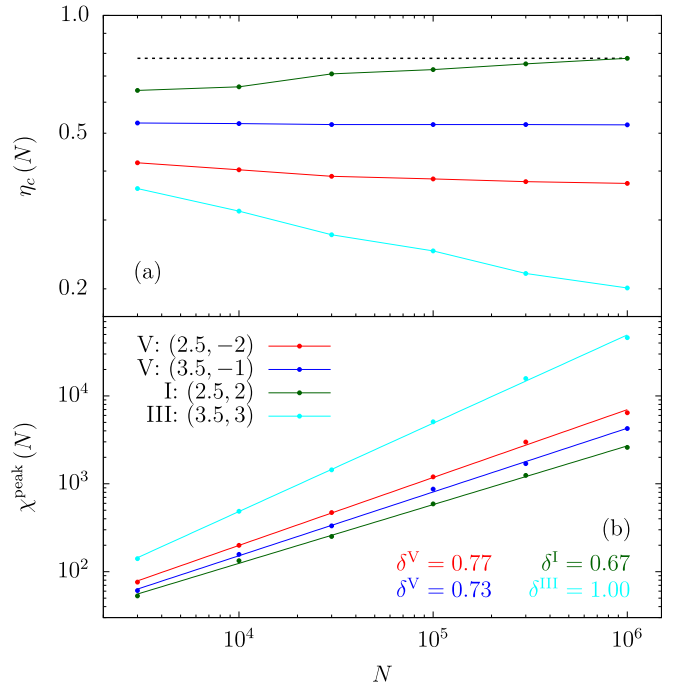


FIG. 7. (a) Effective critical point $\eta_c(N)$ as a function of the network size N for different pairs of values (γ, α) belonging to regions I, III, and V. The dashed horizontal line serves to highlight the slow convergence to 1 of the threshold observed in region I. (b) Maximum of the dynamic susceptibility at the peak, $\chi^{\text{peak}}(N)$, as a function of the network size N for different pairs of values (γ, α) . The exponents δ quoted of the different regions are obtained by means of a linear regression in log-log scale to the form $\chi^{\text{peak}} \sim N^\delta$. Results correspond to the Vicsek model on UCM weighted networks.

is substantially larger in the Vicsek model than in the CBV model, whereas the opposite happens for the rate of growth in region I, being faster in the CBV model. This is due to the fact that, in the Vicsek model, the threshold converges to a maximum value, while in the CBV model it grows without limit.

Finally, in Fig. 7(b) we present the growth of the maximum of the susceptibility at its peak as a function of the network size, for the different pairs of values (γ, α) . A linear regression in logarithmic scale shows the expected power-law dependence $\chi^{\text{peak}}(N) \sim N^\delta$. In contrast with the CBV model, in the Vicsek case the exponent δ seems to depend on α and γ simultaneously.

V. NUMERICAL RESULTS IN REAL WEIGHTED NETWORKS

In order to ascertain the effects of a real weighted topology on flocking dynamics, we have studied the behavior of the Vicsek model on several empirical animal social weighted networks [60]. As weighted substrates, we consider 20 networks reflecting dominance relationships, behavioral activities, sexual interactions, and mating associations in different species (see Table II for references to the network's details). Since some of these networks are directed in nature, in our analysis we have worked with their undirected version, in which weights have been symmetrized, defining

TABLE II. Topological properties of the real weighted networks analyzed. Network size N , average weight $\langle w \rangle$, normalized variance of the weights $\chi_w = \langle w^2 \rangle / \langle w \rangle^2 - 1$, effective threshold of the weighted network version η_c^w , effective threshold of the binary network version η_c^b , and relative difference of the threshold in the weighted over binary networks $\Delta\eta = 1 - \eta_c^w / \eta_c^b$.

Network	N	$\langle w \rangle$	χ_w	η_c^w	η_c^b	$\Delta\eta$
Bison [61]	26	2.76	0.54	0.834	0.854	0.023
Cattle [62]	28	2.30	0.64	0.802	0.843	0.049
Sheep [63]	28	2.66	0.65	0.829	0.855	0.030
Hyenas [64]	36	0.08	0.55	0.866	0.890	0.027
Bats [65]	43	30.62	1.17	0.860	0.885	0.028
Sparrows [66]	46	2.92	1.09	0.748	0.828	0.097
Dolphins 1 [67]	50	0.33	1.16	0.730	0.882	0.172
Lizards [68]	60	0.02	8.10	0.316	0.724	0.564
Squirrels [69]	61	0.14	1.28	0.827	0.872	0.052
Thornbills [70]	62	2.49	0.72	0.868	0.884	0.018
Macaques 1 [71]	62	2.06	0.44	0.851	0.887	0.041
Macaques 2 [72]	78	2.53	0.73	0.862	0.896	0.038
Songbirds [73]	110	0.02	3.03	0.524	0.802	0.347
Ants [74]	113	7.06	1.25	0.858	0.905	0.052
Wildbirds [75]	149	0.07	1.27	0.804	0.852	0.056
Dolphins 2 [76]	151	1.21	0.19	0.813	0.819	0.007
Crickets [77]	161	2.78	1.07	0.481	0.574	0.162
Voles [78]	255	2.19	0.81	0.421	0.518	0.187
Mice [79]	280	4.55	3.93	0.181	0.313	0.422
Sealions [80]	1007	0.03	0.63	0.926	0.939	0.014

$w_{ij}^s = (w_{ij} + w_{ji})/2$. We have also disregarded nodes of zero degree and edges of zero weight. For the simulations, we have set $t_m = 50\,000$ and $T = 500\,000$. In Table II we present a summary of the topological properties of the animal weighted networks considered.

The HMF theory developed in Sec. III cannot be directly applied to real networks, since those are usually correlated

[32] and the relation between the weight of an edge and the degrees at its endpoints is only approximately fulfilled for large networks [38] and difficult to assess in small ones. For this reason, in order to characterize the effects of weights in our empirical networks, we have compared the behavior in the actual weighted network with that of its binary projection, constructed by assigning to all edges a constant weight w_0 , arbitrarily fixed to 1.

In Fig. 8 we present a plot of the order parameter $\phi(\eta)$ (top row) and the dynamic susceptibility $\chi_N(\eta)$ (bottom row) as a function of the noise intensity η for a sample of four real networks, comparing the results for the weighted and binary simulation procedures. As we can see, the effect of the weights in all four cases is to decrease the shape of the order parameter of the weighted networks with respect to the binary version, effectively reducing the degree of order for large values of η . At the same time, we can see that the peak of the dynamic susceptibility is shifted to the left in the weighted case, indicating that the effective threshold in the weighted network, η_c^w , is smaller than in its binary counterpart, η_c^b . This effect is confirmed in the whole set of 20 networks considered, as shown by the relative threshold difference, $\Delta\eta = 1 - \eta_c^w / \eta_c^b$, being always positive, see Table II.

While we do not have an analytical insight about the dependence of the threshold on the topological substrate of the network, an examination of Table II shows that the threshold in the weighted networks is correlated with the weight heterogeneity, as measured by the normalized variance $\chi_w = \langle w^2 \rangle / \langle w \rangle^2 - 1$. Indeed, a closer inspection indicates a stronger correlation between the relative threshold difference $\Delta\eta$ and the variance of weights, which seems to be related by a power-law form $\Delta\eta \sim \chi_w^a$, with an exponent approximately equal to $a = 1.2$, see Fig. 9. This exponent is obtained via linear regression in double logarithmic scale, with a significant Pearson regression coefficient $r = 0.85$.

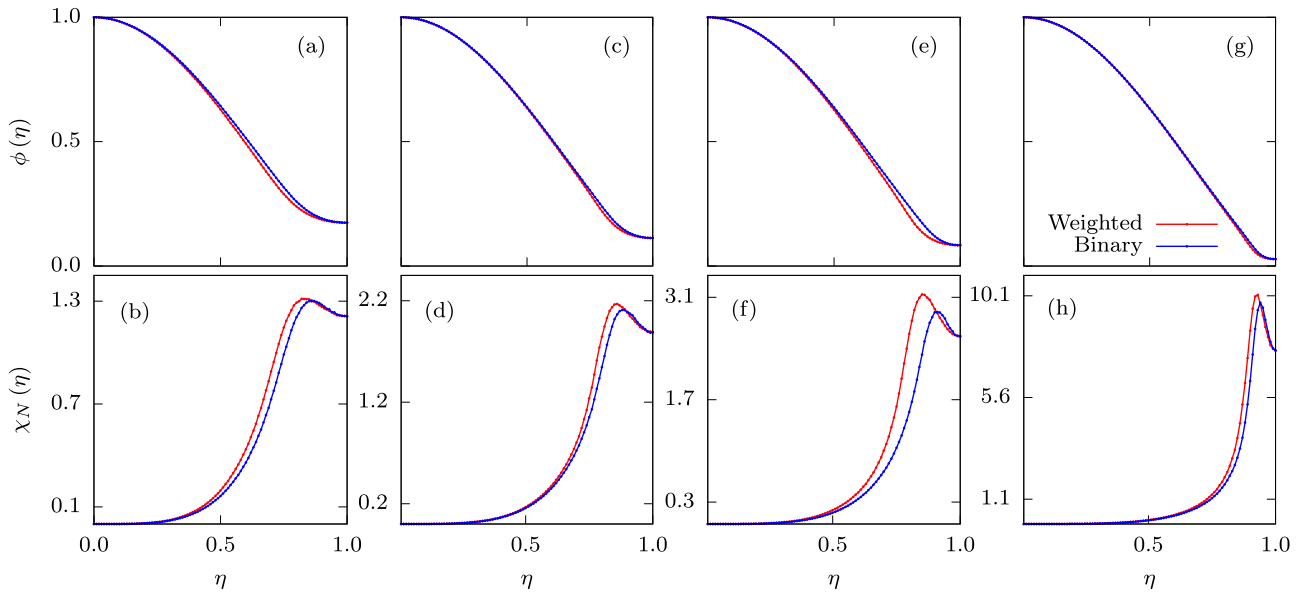


FIG. 8. Order parameter $\phi(\eta)$ (top row) and dynamic susceptibility $\chi_N(\eta)$ (bottom row) as a function of η in the Vicsek model on a sample of four different real animal social weighted networks: [(a) and (b)] Bison, [(c) and (d)] Macaques 1, [(e) and (f)] Ants, and [(g) and (h)] Sealions. A comparison between weighted and binary structures is shown.

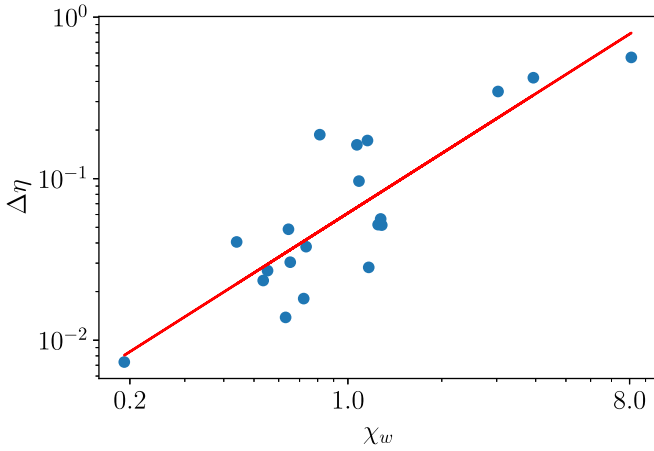


FIG. 9. Relative difference of the weighted and binary thresholds $\Delta\eta$ as a function of the normalized variance of the weights χ_w . A power law relation is denoted by the straight line, $\Delta\eta \sim \chi_w^{1.2}$.

VI. CONCLUSIONS

Social ties can play an important role in shaping the interactions between animals ruling their collective behavior [16]. Indeed, it has been recently shown that a heterogeneous pattern of social interactions, represented in terms of a complex network, can alter the properties of the flocking transition in simple models of collective behavior [22,23]. Here we have presented an extension of previous studies of collective motion mediated by social interactions by considering the weighted nature of social contacts, in which the network topology is enriched by adding a real variable w_{ij} between the connected nodes i and j , representing the intensity of the social contact between this pair of individuals. In this context, we have focused on the effects of a weighted topology on the threshold marking the position of the flocking transition in the classic Vicsek model of collective motion, and in a related model (CBV) which has been shown to behave similarly to the Vicsek model in networks [23]. In the case of a weighted structure depending on the degree of nodes, of the form $w_{ij} = w_0(k_i k_j)^\alpha a_{ij}$, the CBV model can be solved within a heterogeneous mean-field approximation, obtaining an expression of the threshold as a function of the exponent α and the exponent γ of the degree distribution, assumed to have a power-law form $P(k) \sim k^{-\gamma}$. The solution provides a phase diagram in the plane (γ, α) , in which a phase corresponds to a finite threshold and other to a threshold that diverges in the thermodynamic limit. This last phase corresponds to a system that is always ordered in the thermodynamic limit, and therefore very resilient to the effects of external noise. These two behaviors were already observed in the CBV and Vicsek models in nonweighted networks [22,23]. However, in the weighted case, a new phase emerges, in which the threshold actually tends to zero in the thermodynamic limit. This surprisingly corresponds to a system that is always disordered for any amount of noise, however small, and indicates a dynamics extremely susceptible to the effects of external perturbations.

Numerical simulations in the CBV model recover the theoretical predictions of the HMF approximation with good

qualitative accuracy, with the exception of points very close to the boundaries between regions, in which finite-size effects are stronger and larger system sizes than those considered here are necessary. For networks of finite size, we additionally observe the presence of a maximum in the threshold as a function of α for fixed γ . This indicates that a particular weight pattern can provide the maximum resilience against noise perturbations, by maximizing the value of the flocking threshold. At the HMF level, this maximum is obtained for a weight exponent $\alpha = 1/2$. Simulations lead instead to a maximum slightly depending on the degree exponent. Furthermore, simulations of the more realistic Vicsek model yield results that can be understood in terms of the HMF solution of the CBV model, by simply mapping the physical limits of the noise parameters in both models, 1 for the Vicsek model and infinity for the CBV model. With this mapping, simulations of the Vicsek model closely follow the prediction and results obtained for the CBV model. We recover in particular the presence of a region with a vanishing threshold, and extremely susceptible to noise effects.

We finally consider the behavior of the Vicsek model in real weighted networks representing social interactions between different animal species. Lacking a theory for real networks, we observe that the threshold of the weighted structures is in general smaller than the one observed in the binary (nonweighted) version of the same networks. This indicates that the weighted pattern in real social interactions is actually not beneficial for a flock of animals, since it reduces the flocking threshold and thus renders the group more susceptible to breaking in the presence of noise fluctuations. The relative difference between the weighted and nonweighted thresholds is empirically observed to depend on the degree of heterogeneity of the weight pattern, in a functional form that can be approximated by a power law. This observation indicates that more heterogeneous patterns of weights, with some connections much stronger than others, is again detrimental to maintain the flock structure of the animal group.

The results presented here strengthen the equivalence between the Vicsek and CBV model in networks [23] and highlight the important effects that a social network of interactions can have on the flocking structure of social animals. Most interestingly, they show that in some cases the presence of a weight pattern can be counterproductive for a flocking species, by reducing their resilience to noise or by destroying the flocking phase altogether. The presence of such weight pattern must thus be attributed some other adaptive benefit, that overcomes the worsened flocking performance. Future venues for theoretical work regarding the models proposed here could consider going beyond HMF and applying a quenched mean-field theory, considering the static structure of the network in terms of the adjacency matrix [81,82], or considering the actual dynamic nature of social networks by implementing the models on top of temporal networks [83].

ACKNOWLEDGMENTS

We acknowledge financial support from the Spanish MCIN/AEI/10.13039/501100011033, under project No. PID2019-106290GB-C21. We thank Jordi Torrents for helpful comments and discussions.

- [1] S. Camazine, J.-L. Deneubourg, N. R. Franks, J. Sneyd, G. Theraula, and E. Bonabeau, *Self-organization in Biological Systems*, Princeton Studies in Complexity (Princeton University Press, Princeton, NJ, 2001).
- [2] D. J. Sumpter, *Collective Animal Behavior* (Princeton University Press, NJ, 2010).
- [3] D. J. T. Sumpter, The principles of collective animal behaviour, *Philos. Trans. R. Soc. B* **361**, 5 (2006).
- [4] T. Vicsek and A. Zafeiris, Collective motion, *Phys. Rep.* **517**, 71 (2012).
- [5] I. Giardina, Collective behavior in animal groups: theoretical models and empirical studies, *HFSP J.* **2**, 205 (2008).
- [6] A. Cavagna, I. Giardina, and T. S. Grigera, The physics of flocking: Correlation as a compass from experiments to theory, *Phys. Rep.* **728**, 1 (2018).
- [7] F. Romero-Ferrero, M. G. Bergomi, R. C. Hinz, F. J. H. Heras, and G. G. de Polavieja, idtracker.ai: Tracking all individuals in small or large collectives of unmarked animals, *Nat. Methods* **16**, 179 (2019).
- [8] T. Walter and I. D. Couzin, Trex, a fast multi-animal tracking system with markerless identification, and 2d estimation of posture and visual fields, *eLife* **10**, e64000 (2021).
- [9] I. Aoki, A simulation study on the schooling mechanism in fish, *Bull. Jpn. Soc. Sci. Fisheries* **48**, 1081 (1982).
- [10] C. W. Reynolds, Flocks, herds and schools: A distributed behavioral model, *SIGGR. Comput. Graph.* **21**, 25 (1987).
- [11] I. Couzin, J. Krause, R. James, G. Ruxton, and N. Franks, Collective memory and spatial sorting in animal groups, *J. Theor. Biol.* **218**, 1 (2002).
- [12] M. Ballerini, N. Cabibbo, R. Candelier, A. Cavagna, E. Cisbani, I. Giardina, V. Lecomte, A. Orlandi, G. Parisi, A. Procaccini, M. Viale, and V. Zdravkovic, Interaction ruling animal collective behavior depends on topological rather than metric distance: Evidence from a field study, *Proc. Natl. Acad. Sci. U.S.A.* **105**, 1232 (2008).
- [13] F. Ginelli and H. Chaté, Relevance of Metric-Free Interactions in Flocking Phenomena, *Phys. Rev. Lett.* **105**, 168103 (2010).
- [14] J. E. Herbert-Read, A. Perna, R. P. Mann, T. M. Schaerf, D. J. T. Sumpter, and A. J. W. Ward, Inferring the rules of interaction of shoaling fish, *Proc. Natl. Acad. Sci. U.S.A.* **108**, 18726 (2011).
- [15] D. Croft, R. James, and J. Krause, *Exploring Animal Social Networks* (Princeton University Press, Princeton, NJ, 2008).
- [16] H. Ling, G. E. McIvor, K. van der Vaart, R. T. Vaughan, A. Thornton, and N. T. Ouellette, Costs and benefits of social relationships in the collective motion of bird flocks, *Nat. Ecol. Evol.* **3**, 943 (2019).
- [17] M. Aldana, V. Dossetti, C. Huepe, V. M. Kenkre, and H. Larralde, Phase Transitions in Systems of Self-Propelled Agents and Related Network Models, *Phys. Rev. Lett.* **98**, 095702 (2007).
- [18] J. A. Pimentel, M. Aldana, C. Huepe, and H. Larralde, Intrinsic and extrinsic noise effects on phase transitions of network models with applications to swarming systems, *Phys. Rev. E* **77**, 061138 (2008).
- [19] A. Sekunda, M. Komareji, and R. Bouffanais, Interplay between signaling network design and swarm dynamics, *Net. Sci.* **4**, 244 (2016).
- [20] N. W. F. Bode, A. J. Wood, and D. W. Franks, Social networks and models for collective motion in animals, *Behav. Ecol. Sociobiol.* **65**, 117 (2011).
- [21] N. W. Bode, A. J. Wood, and D. W. Franks, The impact of social networks on animal collective motion, *Anim. Behav.* **82**, 29 (2011).
- [22] M.-C. Miguel, J. T. Parley, and R. Pastor-Satorras, Effects of Heterogeneous Social Interactions on Flocking Dynamics, *Phys. Rev. Lett.* **120**, 068303 (2018).
- [23] M.-C. Miguel and R. Pastor-Satorras, Scalar model of flocking dynamics on complex social networks, *Phys. Rev. E* **100**, 042305 (2019).
- [24] P. Clusella and R. Pastor-Satorras, Phase transitions on a class of generalized Vicsek-like models of collective motion, *Chaos* **31**, 043116 (2021).
- [25] M. Aldana and C. Huepe, Phase transitions in self-driven many-particle systems and related non-equilibrium models: A network approach, *J. Stat. Phys.* **112**, 135 (2003).
- [26] V. Mwaffo, R. P. Anderson, and M. Porfiri, Collective dynamics in the vicsek and vectorial network models beyond uniform additive noise, *J. Nonlin. Sci.* **25**, 1053 (2015).
- [27] M. Porfiri and G. Ariel, On effective temperature in network models of collective behavior, *Chaos* **26**, 043109 (2016).
- [28] T. Vicsek, A. Czirok, E. Ben-Jacob, I. Cohen, and O. Shochet, Novel Type of Phase Transition in a System of Self-Driven Particles, *Phys. Rev. Lett.* **75**, 1226 (1995).
- [29] F. Ginelli, The physics of the Vicsek model, *Eur. Phys. J.: Spec. Top.* **225**, 2099 (2016).
- [30] G. Grégoire and H. Chaté, Onset of Collective and Cohesive Motion, *Phys. Rev. Lett.* **92**, 025702 (2004).
- [31] J. Gao, S. Havlin, X. Xu, and H. E. Stanley, Angle restriction enhances synchronization of self-propelled objects, *Phys. Rev. E* **84**, 046115 (2011).
- [32] M. Newman, *Networks: An Introduction* (Oxford University Press, Inc., New York, 2010).
- [33] D. Lusseau, The emergent properties of a dolphin social network, *Proc. R. Soc. Lond B* **270**, S186 (2003).
- [34] T. G. Manno, Social networking in the Columbian ground squirrel, *Spermophilus columbianus*, *Anim. Behav.* **75**, 1221 (2008).
- [35] A.-L. Barabási and R. Albert, Emergence of scaling in random networks, *Science* **286**, 509 (1999).
- [36] A. Czirok, A.-L. Barabási, and T. Vicsek, Collective Motion of Self-Propelled Particles: Kinetic Phase Transition in One Dimension, *Phys. Rev. Lett.* **82**, 209 (1999).
- [37] M. E. J. Newman, Analysis of weighted networks, *Phys. Rev. E* **70**, 056131 (2004).
- [38] A. Barrat, M. Barthélemy, R. Pastor-Satorras, and A. Vespignani, The architecture of complex weighted networks, *Proc. Natl. Acad. Sci. U.S.A.* **101**, 3747 (2004).
- [39] M. Barthélemy, A. Barrat, R. Pastor-Satorras, and A. Vespignani, Characterization and modeling of weighted networks, *Physica A* **346**, 34 (2005).
- [40] Y. Gang, Z. Tao, W. Jie, F. Zhong-Qian, and W. Bing-Hong, Epidemic spread in weighted scale-free networks, *Chin. Phys. Lett.* **22**, 510 (2005).
- [41] M. Karsai, R. Juhász, and F. Iglói, Nonequilibrium phase transitions and finite-size scaling in weighted scale-free networks, *Phys. Rev. E* **73**, 036116 (2006).
- [42] M. Deijfen, Epidemics and vaccination on weighted graphs, *Math Biosci.* **232**, 57 (2011).
- [43] A. Baronchelli, C. Castellano, and R. Pastor-Satorras, Voter models on weighted networks, *Phys. Rev. E* **83**, 066117 (2011), 1011.2395.

- [44] S. B. Rosenthal, C. R. Twomey, A. T. Hartnett, H. S. Wu, and I. D. Couzin, Revealing the hidden networks of interaction in mobile animal groups allows prediction of complex behavioral contagion, *Proc. Natl. Acad. Sci. U.S.A.* **112**, 4690 (2015).
- [45] T. Xue, X. Li, P. Grassberger, and L. Chen, Swarming transitions in hierarchical societies, *Phys. Rev. Res.* **2**, 042017(R) (2020).
- [46] G. Ariel, A. Ayali, A. Be'er, and D. Knebel, Variability and heterogeneity in natural swarms: Experiments and modeling, in *Active Particles, Volume 3, Advances in Theory, Models, and Applications*, Modeling and Simulation in Science, Engineering and Technology (Springer, Berlin, 2022), pp. 1–33.
- [47] R. Pastor-Satorras and A. Vespignani, Epidemic Spreading in Scale-Free Networks, *Phys. Rev. Lett.* **86**, 3200 (2001).
- [48] A. Barrat, M. Barthélemy, and A. Vespignani, *Dynamical Processes on Complex Networks*, 1st ed. (Cambridge University Press, New York, 2008).
- [49] S. N. Dorogovtsev, A. V. Goltsev, and J. F. F. Mendes, Critical phenomena in complex networks, *Rev. Mod. Phys.* **80**, 1275 (2008).
- [50] R. Pastor-Satorras, C. Castellano, P. Van Mieghem, and A. Vespignani, Epidemic processes in complex networks, *Rev. Mod. Phys.* **87**, 925 (2015).
- [51] H. Chen, C. Shen, G. He, H. Zhang, and Z. Hou, Critical noise of majority-vote model on complex networks, *Phys. Rev. E* **91**, 022816 (2015).
- [52] C. Castellano and R. Pastor-Satorras, Zero temperature Glauber dynamics on complex networks, *J. Stat. Mech.: Theory Exp.* (2006) P05001.
- [53] R. Pastor-Satorras, A. Vázquez, and A. Vespignani, Dynamical and Correlation Properties of the Internet, *Phys. Rev. Lett.* **87**, 258701 (2001).
- [54] M. Abramowitz and I. A. Stegun, *Handbook of Mathematical Functions* (Dover, New York, 1972).
- [55] M. Boguñá, C. Castellano, and R. Pastor-Satorras, Langevin approach for the dynamics of the contact process on annealed scale-free networks., *Phys. Rev. E* **79**, 036110 (2009).
- [56] M. Boguñá, R. Pastor-Satorras, and A. Vespignani, Cut-offs and finite size effects in scale-free networks, *Eur. Phys. J. B* **38**, 205 (2004).
- [57] M. Catanzaro, M. Boguñá, and R. Pastor-Satorras, Generation of uncorrelated random scale-free networks, *Phys. Rev. E* **71**, 027103 (2005).
- [58] S. C. Ferreira, C. Castellano, and R. Pastor-Satorras, Epidemic thresholds of the susceptible-infected-susceptible model on networks: A comparison of numerical and theoretical results, *Phys. Rev. E* **86**, 041125 (2012).
- [59] C. Castellano and R. Pastor-Satorras, On the numerical study of percolation and epidemic critical properties in networks, *Eur. Phys. J. B* **89**, 243 (2016).
- [60] P. Sah, J. Méndez, and S. Bansal, A multi-species repository of social networks, *Sci. Data* **6**, 44 (2019).
- [61] D. F. Lott, Dominance relations and breeding rate in mature male American bison, *Zeitschr. Tierpsychol.* **49**, 418 (1979).
- [62] C. C. Hass, Social status in female bighorn sheep (*Ovis canadensis*): Expression, development and reproductive correlates, *J. Zool.* **225**, 509 (1991).
- [63] M. W. Schein and M. H. Fohrman, Social dominance relationships in a herd of dairy cattle, *Br. J. Anim. Behav.* **3**, 45 (1955).
- [64] K. E. Holekamp, J. E. Smith, C. C. Strelhoff, R. C. Van Horn, and H. E. Watts, Society, demography and genetic structure in the spotted hyena, *Molec. Ecol.* **21**, 613 (2012).
- [65] A. Silvis, A. B. Kniowski, S. D. Gehrt, and W. M. Ford, Roosting and foraging social structure of the endangered Indiana bat (*Myotis sodalis*), *PLoS One* **9**, e96937 (2014).
- [66] D. Shizuka, A. S. Chaine, J. Anderson, O. Johnson, I. M. Laursen, and B. E. Lyon, Across-year social stability shapes network structure in wintering migrant sparrows, *Ecol. Lett.* **17**, 998 (2014).
- [67] T. N. Hunt, S. J. Allen, L. Bejder, and G. J. Parra, Assortative interactions revealed in a fission–fusion society of Australian humpback dolphins, *Behav. Ecol.* **30**, 914 (2019).
- [68] C. M. Bull, S. S. Godfrey, and D. M. Gordon, Social networks and the spread of Salmonella in a sleepy lizard population, *Molec. Ecol.* **21**, 4386 (2012).
- [69] J. E. Smith, D. A. Gamboa, J. M. Spencer, S. J. Travenick, C. A. Ortiz, R. D. Hunter, and A. Sih, Split between two worlds: Automated sensing reveals links between above- and belowground social networks in a free-living mammal, *Philos. Trans. R. Soc. B* **373**, 20170249 (2018).
- [70] D. R. Farine and P. J. Milburn, Social organisation of thornbill-dominated mixed-species flocks using social network analysis, *Behav. Ecol. Sociobiol* **67**, 321 (2013).
- [71] Y. Takahata, Diachronic changes in the dominance relations of adult female Japanese monkeys of the Arashiyama B group, in *The Monkeys of Arashiyama*, edited by L. M. Fedigan and P. J. Asquith (State University of New York Press, Albany, 1991), pp. 123–139.
- [72] K. Balasubramaniam, B. Beisner, J. Guan, J. Vandeleeest, H. Fushing, E. Atwill, and B. McCowan, Social network community structure and the contact-mediated sharing of commensal *E. coli* among captive rhesus macaques (*Macaca mulatta*), *PeerJ* **6**, e4271 (2018).
- [73] J. S. Adelman, S. C. Moyers, D. R. Farine, and D. M. Hawley, Feeder use predicts both acquisition and transmission of a contagious pathogen in a North American songbird, *Proc. R. Soc. B* **282**, 20151429 (2015).
- [74] D. P. Mersch, A. Crespi, and L. Keller, Tracking individuals shows spatial fidelity is a key regulator of ant social organization, *Science* **340**, 1090 (2013).
- [75] J. A. Firth and B. C. Sheldon, Experimental manipulation of avian social structure reveals segregation is carried over across contexts, *Proc. R. Soc. B* **282**, 20142350 (2015).
- [76] S. Gazda, S. Iyer, T. Killingback, R. Connor, and S. Brault, The importance of delineating networks by activity type in bottlenose dolphins (*Tursiops truncatus*) in Cedar Key, Florida, *R. Soc. Open Sci.* **2**, 140263 (2015).
- [77] D. N. Fisher, R. Rodríguez-Muñoz, and T. Tregenza, Comparing pre- and post-copulatory mate competition using social network analysis in wild crickets, *Behav. Ecol.* **27**, 912 (2016).
- [78] S. Davis, B. Abbasi, S. Shah, S. Telfer, and M. Begon, Spatial analyses of wildlife contact networks, *J. R. Soc. Interface* **12**, 20141004 (2015).
- [79] P. C. Lopes, P. Block, and B. König, Infection-induced behavioural changes reduce connectivity and the potential for disease spread in wild mice contact networks, *Sci. Rep.* **6**, 31790 (2016).

- [80] Z. A. Schakner, M. B. Petelle, M. J. Tennis, B. K. Van der Leeuw, R. T. Stansell, and D. T. Blumstein, Social associations between California sea lions influence the use of a novel foraging ground, *R. Soc. Open Sci.* **4**, 160820 (2017).
- [81] J. P. Gleeson, High-Accuracy Approximation of Binary-State Dynamics on Networks, *Phys. Rev. Lett.* **107**, 068701 (2011).
- [82] F. Huang, H. Chen, and C. Shen, Quenched mean-field theory for the majority-vote model on complex networks, *Europhys. Lett.* **120**, 18003 (2017).
- [83] P. Holme and J. Saramäki, Temporal networks, *Phys. Rep.* **519**, 97 (2012).